Production of J/Ψ mesons in p–Pb collisions at the Large Hadron Collider

Bachelor thesis
by
Madeleine Petersson Sjögren

Supervised by
David Silvermyr

LUND
UNIVERSITY

DIVISION OF PARTICLE PHYSICS
SPRING 2015

Abstract

Data from p–Pb collisions reconstructed with the ALICE experiment at $\sqrt{s} = 5.02$ TeV is analyzed to study J/Ψ production (a possible Quark-Gluon Plasma signal) in different p_{T} ranges. Results obtained by studying the invariant mass distribution via the dielectron decay channel show a significant J/Ψ yield from approximately $p_{\mathrm{T}} > 2$ GeV/c with statistics up to about 10 GeV/c. The signal is observed via Unlike-Sign pairs, and the combinatorial background is estimated via Like-Sign pairs.

Populärvetenskaplig sammanfattning

Partikelfysik eller högenergifysik är studiet av de minsta partiklarna i all materia: elementarpartiklarna och deras växelverkan med varandra. Högenergifysikforskning bedrivs framförallt genom att accelerera partiklar till höga energier och låta dem kollidera, antingen med ett fixerat mål eller med en annan skur av partiklar. Kärnfysik å andra sidan är studiet av de tunga atomkärnorna som består av mindre partiklar. Mixar man högenergifysik med kärnfysik får man tungjonsfysik där man studerar beteendet hos kärnmateria i energiregimer typiska för högenergifysik.

Den centrala teorin för partikel- och tungjonsfysik är Standardmodellen. Denna teori delar upp de kända elementarpartiklarna som all materia är uppbyggd av i tre olika familjer. Förutom materiepartiklarna berättar teorin om Bosonerna, som är bärare av de fundamentala krafterna: Starka, Elektromagnetiska och Svaga kraften. Var materie-familj består av två kvarkar och två leptoner. Kvarkarna är de minsta beståndsdelarna som bygger upp mer komplexa partiklar och deras namn är Upp, Ned, Charm, Sär, Topp och Botten. De är alla färgladdade och hålls samman av bosontypen gluoner för att bilda sammansatta partiklar: hadroner. Vidare är bosontypen foton ansvarig för förmedlandet av den elektromagnetiska kraften medan den svaga kraften förmedlas av Z^0 och $W^{+/-}$ bosoner. Leptonerna är elektroner, myoner och tauoner, som alla bär elektrisk laddning, och deras vardera associerade neutrala neutrino. För var partikel i teorin finns även en antipartikel. Två välkända hadroner är protonen och neutronen. De består av tre kvarkar var som fästes i varandra med hjälp av gluonerna. Kärnor inuti atomer är i sin tur sammansatta av flera protoner och neutroner.

Några av världens allra största laboratorier används för studiet av dessa stora kärnor och elementära partiklar, så kallade partikelacceleratorer. Idag finns partikelacceleratorer runt om i världen vid olika forskningscentra och en av de mest kända är the Large Hadron Collider (LHC) vid forskningcentrat CERN i centrala Europa. För att ta reda på hur materian i kärnorna, eller de elementära partiklarna beter sig studeras utkomsten av kollisionerna. För detta ändamål har stora detektorer byggts för att detektera och rekonstruera händelseförloppet hos kollisionerna och de partiklar och sönderfallsprodukter som bildas. När tunga kärnor kolliderar har man funnit att ett alldeles speciellt tillstånd av materia bildas, ett så kallat Kvark-Gluon Plasma. Tillståndet utmärker sig genom att kvarkar och gluoner befinner sig i ett friare tillstånd, som man vill studera ytterligare. Man tror att det var just detta tillstånd som var det dominanta under en kort stund vid universums skapelse, precis efter Big Bang!

Den marginala utbredningen och den korta livslängden hos Kvark Gluon Plasmat gör det omöjligt att detektera direkt. För att säkerställa dess existens och identifiera dess egenskaper försöker man mäta olika Kvark Gluon Plasma signaler. En möjlig sådan signal är produktionen av J/Ψ partiklar relativt vad som observerats i proton-proton kollisioner. J/Ψ partikeln är en hadron sammansatt av en c- och en anti-c-kvark. I denna uppsats har proton-kärna kollisioner analyserats för att studera produktionen av J/Ψ partikeln.

Contents

Introduction

One objective of today's experiments with high energy heavy-ion collisions is to identify and study the Quark-Gluon Plasma (QGP). The state is special because it exhibits properties not found in any other form of matter and it is believed that the QGP state was present in the very early universe, just after the Big Bang [1]. By colliding heavy nuclei, conditions similar to those of the early universe are created in the laboratory. In the QGP quarks, the smallest components of hadronic matter, and gluons, particles associated with the interquark forces, can move outside a normal hadronic radii.

The study of QGP is crucial to understand the strong interactions of quarks and gluons. However, the detection of QGP and its properties are not yet fully understood. As created in the laboratory QGP exists for very short times (a few fm/c) and extends to a size of a few fm which makes its detection and characterization a challenging objective.

In this thesis, one possible signal of QGP is treated: the J/Ψ suppression. For decades this probe has been suggested as a possible signal of QGP formation able to probe it at an early stage of its formation. However, depending on the type of collision and collision energy J/Ψ suppression can also be explained by effects that are understood not to arise from the QGP [2]. Additionally it has lately been realised that effects due to QGP formation might instead lead to an enhanced J/Ψ production at higher energies [3]. Therefore the J/Ψ probe has become a more complicated and less conclusive signal than originally thought in the search for QGP and it needs to be studied from many different aspects. The aim of this thesis is to study the production of J/Ψ in proton–lead collisions through an invariant mass analysis.

1. Theory

In this section some concepts of modern particle physics are introduced. A brief overview of the Standard Model and the theory of the strong force (QCD) is given. This is followed by a discussion of the QGP state and one of its possible signals. For a more complete overview see e.g. Ref. [4] for the Standard Model and Ref. [5] for QCD and the QGP state of matter.

The Standard Model

The Standard Model (SM) aims to explain all known particle physics in terms of a few fundamental particles and forces. The theory is very good at categorizing particles by their properties into subgroups and has been effective in predicting the discovery of new particles. Fig. 1.1 shows three subgroups of particles in the Standard Model: quarks, leptons and bosons.

The Standard Model consists of fundamental particles grouped into two different classes: integer-spin particles (bosons) and half-integer-spin particles (fermions). All matter is made up of 12 fermions: six leptons and six quarks and their respective antiparticles. Some of the leptons carry electric charge while quarks carry both electric and color charge. The quarks come in six different flavours: up, down, charm, strange, top and bottom. Bosons are mediators of the fundamental forces: the electromagnetic force is mediated by *photons*, the weak force by the $W^{+/-}$ and Z^0 bosons and the strong force by the *gluons*. The fourth fundamental force is gravity but a mediator of this force has not yet been found. Photons interact with electrically charged particles and this interaction is extensively described by Quantum Electrodynamics (QED). The $W^{+/-}$ and Z^0 bosons interact weakly with all particles that carry weak isospin, including all fermions but also the $W^{+/-}$ and Z^0 bosons themselves. The gluons interact exclusively with color charged particles: quarks and gluons, which are collectively referred to as partons. Hadrons are composite particles made up of partons and the two possible combinations of bound states of partons are baryons, which consist of three valence quarks, and mesons, which consist of a quark and an antiquark. All hadrons are color neutral. "Free" quarks have never been observed isolated from other quarks, hence the color of the confined quarks cancel out.

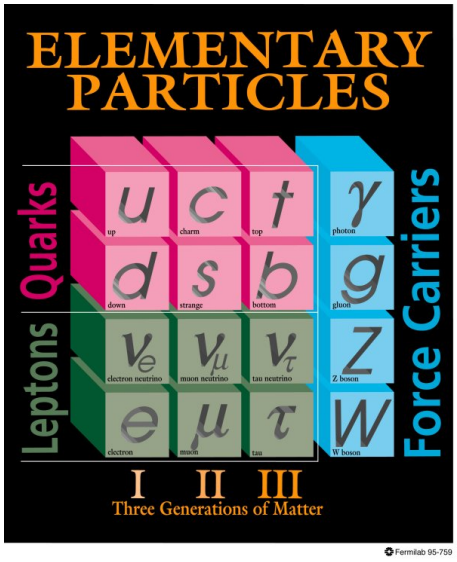

Figure 1.1: The Standard Model of particle physics. There are three generations of matter particles (**I**, **II** and **III**) each containing two quarks and two leptons. An additional fourth column shows the force mediators. [6]

Quantum Chromodynamics

Quantum Chromodynamics (QCD) is the theory of the strong interaction between quarks. It is governed by the running coupling constant α_s, which is almost constant for high energies and increases for lower energies. QCD has similarities to Quantum Electrodynamics (QED), which describes the electromagnetic interaction between electrically charged particles. Both theories describe forces mediated by bosons and are in good agreement with experiments today. However, while QED has been tested extensively, QCD has proven to be more complicated. The major difference between the two theories is the existence of color charge and its implications.

Unlike photons, which are electrically neutral, gluons themselves carry a nonzero color charge which makes it possible for the gluon to interact with other gluons and also with itself, through quantum fluctuations. The gluon-gluon interaction lead to properties of the strong interaction called *color confinement* and *asymptotic freedom*. The color confinement of quarks implies that composite states of quarks have zero color charge and hence that quarks cannot be observed as isolated free particles. Due to quantum fluctuations gluons emit and absorb new gluon pairs which enables anti-screening of the original color charge [7]. At the inside of a hadron it seems as though quarks are relatively free to move about in a sea of quarks and antiquarks but as the distance between the quarks is increased the strong force is also enhanced. However, at high enough energies the strong force is weakened. [7].

The total momentum of a hadron is shared by all the partons that the hadron is made of. Their momentum distributions are given by Parton Distribution Functions (PDFs), which represent the probability of finding a parton with a fraction x of the longitudinal momentum of the hadron at resolution scale Q^2 [5]. For heavy nuclei the PDFs are modified since one nucleus is made up of several hadrons.

Hadronic decay and short-lived particles

The majority of all hadrons are unstable particles, meaning that if they can decay they will do so. Preferably a particle decays via the strong interaction, in which the quark number is conserved. If such a decay is not possible, the particle will instead decay electromagnetically or weakly. If possible, a hadron will decay shortly after being created. Hence, the particle is *short-lived*, as opposed to a *long-lived* or *stable* one. Due to their short lifetimes short-lived particles, even when created with a velocity close to the speed of light, are able to travel only very short distances, of the order 10^{-15} m (the approximate diameter of a proton) before decaying [4]. The implication of the short distance between a collision creating a short-lived particle and the point where it decays is that the particle itself cannot be detected, instead one has to study the decay products of it.

The invariant mass (also referred to as the rest mass) of a particle is the mass that remains constant under Lorentz transformations. Knowing the momentum and energy of a particle's decay products, its invariant mass can be reconstructed. The invariant mass, m_{inv}, is defined as

$$m_{\text{inv}}^2 c^2 = \left(\frac{E}{c}\right)^2 - \vec{p}^2 \tag{1.0.1}$$

where E is the total energy and $\vec{p}$ is the total momentum of the decay products. So, for a decay into two particles (1 and 2) the invariant mass is defined as

$$m_{\text{inv}}^2 c^2 = \left(\frac{E_1 + E_2}{c}\right)^2 - (\vec{p}_1 + \vec{p}_2)^2 \,. \tag{1.0.2}$$

Hence, by measuring the energies and the momentum vectors of the decay products the mass of the mother particle can be determined.

Quark-Gluon Plasma

In ordinary matter, hadrons have a finite spatial extension due to the color confinement of QCD. However, at sufficiently high densities this extension can be increased to that of a nucleus, meaning that the quarks and gluons of a hadron are no longer limited by the hadronic radii but rather by the nucleus radii [7]. Under conditions of great pressure and temperature the strong force between quarks and gluons is weakened and a phase transition occurs. The new state is a deconfined state of strongly interacting particles referred to as Quark-Gluon Plasma (QGP). The mechanism of deconfinement is provided by screening of the color charge which implies that the color potential becomes short-ranged [7]. In QGP the relevant degrees of freedom are partons rather than hadrons. It is believed that this state of matter was the dominant one in the primordial universe and therefore the study of the QGP may give insight to what the early universe looked like [1].

Conditions similar to those of the early universe are created by colliding heavy atomic nuclei at particle accelerators. The collisions give rise to high enough energy densities to create a fireball in which the QGP forms [8]. As the fireball expands in space the density is decreased and finally the matter in the QGP hadronizes. The period of time during which this happens is referred to as the *freeze-out* phase. The plasma is expected to have a very short lifetime, of the order of a few fm, and a 5 to 10 fm/c extension in space, which implies great challenges for studying the QGP [9].

The QGP is expected to manifest itself through different signatures such as supression of highly energetic jets, collective particle motion, enhancement of strange particle production and various probes of deconfinement [10]. One such type of probe or signal of deconfinement that has been proposed is J/Ψ production, and this is the only signature of the QGP to be treated in this thesis.

J/Ψ suppression as a signal of QGP

The J/Ψ particle is a short-lived particle with one charm and one anti-charm quark (c and $\bar{c}$) as constituents. It was discovered separately by two different experiments in 1974; one at Brookhaven National Laboratory (BNL) and the other at Stanford Linear Accelerator Laboratory (SLAC). The two research groups named the particle differently, BNL named it J while SLAC named it Ψ, hence the particle got the name J/Ψ. Since J/Ψ has one charm and one anti-charm quark the total charm of the particle is zero. One says that it has *hidden charm* as opposed to *open charm*. Bound states of $c\bar{c}$ are collectively called charmonium.

In 6% of all cases the J/Ψ decays to electron-positron pairs ($e\bar{e}$) and in 6 % of all cases to muon-anti-muon pairs ($\mu\bar{\mu}$) [11]. These decay modes of J/Ψ and its well established mass of 3.1 GeV/c^2 gives the detection of the particle a narrow and well recognized peak that it is used as a calibration marker in experiments such as ATLAS and CMS [12].

J/Ψ is created in high-energy collisions where hard parton-parton interaction leads to the production of $c\bar{c}$ pairs that form J/Ψ particles [13]. Due to the large mass of the c-quarks the confined state is produced within a short time after the collision and its evolution can probe the state of matter in the early stage of the collision. [7]. The original idea was that if the J/Ψ finds itself in a deconfined state of matter, such as QGP, the screening of the color charge is predicted to reduce the attraction between c and $\bar{c}$ so that the binding between them is weakened and eventually the pair disintegrates [13]. Once the hadronization of the plasma occurs the c and $\bar{c}$ have lost each other and formed hadrons with open charm, such as the D mesons (D^0 and $D^{+/-}$), and the ratio between hidden charm and open charm is decreased. Hence a suppression of the observed J/Ψ signal can reveal the formation of QGP.

Following the reasoning above the suppression of J/Ψ has been proposed as a signature for QGP formed in heavy-ion collisions [13]. Since its formulation, the idea has been investigated in experiments with heavy ion collisions, both at CERN's Super Proton Synchrotron (SPS) and at Brookhaven's Relativistic Heavy-Ion Collider (RHIC) [3]. However, some J/Ψ suppression results

can also be explained by Cold Nuclear Matter (CNM) effects not necessarily related to the QGP. Therefore, the suppression of J/Ψ might not at all be an indication of a QGP state, which makes the outcome of suppressed J/Ψ harder to analyze.

In heavy-ion collisions the yield of J/Ψ is expected to be lower than the corresponding yield expected by a superposition of proton-proton collisions. However, it has also been proposed that at high enough energies the large amount of charm quarks in the QGP may lead to (re)generation of charmonium states by statistical recombination of charm quarks, as the QGP cools down. Hence, this would lead to the unavoidable prediction that instead of suppression of J/Ψ in heavy-ion collisions the charmonium production is actually enhanced at the higher collision energies (or at least the suppression is reduced) due to the QGP formation. The effect is supposed to arise especially at low transverse momentum (p_{T}) [2], see [sec. 2, p. 10] for definition of p_{T}.

In order to establish whether the signal is suppressed or enhanced, heavy-ion collisions have been compared to elementary proton collisions at the same center of mass energy. In the experiments conducted at CERN, more J/Ψ particles than expected were produced in heavy-ion collisions compared to proton-proton collisions, supposedly because of recombination processes of J/Ψ that occur at the freeze-out phase of QGP. [3] However, in order to better decouple CNM effects from those of the QGP-state, proton-nucleus collisions have recently been recorded at CERN. [2]. The hope is that studying J/Ψ production in p–Pb collisions will help clarify the situation and in particular the results observed in Pb–Pb collisions.

2. Heavy-Ion Collisions

In this section some variables used to study heavy-ion collisions are introduced. For a more thorough overview see Ref. [14]. Heavy-ion collision experiments have been conducted at the SPS at CERN, RHIC at BNL and LHC at CERN, creating sufficiently high energy densities to produce QGP by colliding high-energy gold or lead nuclei [1].

The field of relativistic heavy-ion collisions is interdisciplinary in the sense that it connects high-energy physics with nuclear physics. Typically, high-energy physics deals with the interactions that occur when elementary particles (leptons and quarks) are collided. Nuclear physics however, deals with the interactions of the extended and more complicated nuclei that are described by effective models and in heavy-ion collisions a large number of particles are produced (large multiplicities) [14].

Useful variables

In relativistic heavy-ion collisions at the LHC the energy per nucleon in the center of mass frame is several thousand times larger than the individual nucleon mass. Particles that interact with particles of another nucleus in a collision are referred to as *participants* whereas particles that don't are called *spectators*, see Fig. 2.1. The dominant process in high-energy collisions is inelastic scattering between the participants. As nuclei are accelerated to relativistic speeds they are Lorentz contracted before the collision. At the time of collision, hard and soft interactions occur between the participants. The hard collisions happen when partons carrying a large fraction of momentum interact, resulting in high p_{T} hadrons and heavy quarks [5]. Soft collisions are interactions between color fields with smaller fractions of momentum, forming a collective partonic medium in which the strong force is dominant, resulting in the creation of quarks, antiquarks and gluon pairs. The partonic medium is extremly dense and hot and has been found to have liquid-like properties such that it expands in space when undergoing the phase transition to QGP. As the QGP expands in space it cools down and finally reaches the *freeze-out* phase in which quarks and gluons are confined forming hadrons [5].

To study the events in a collision and the formation of the QGP the distribution of particles formed in the freeze-out phase, as well as particles from the pre-freeze-out phase (such as direct photons), are studied.

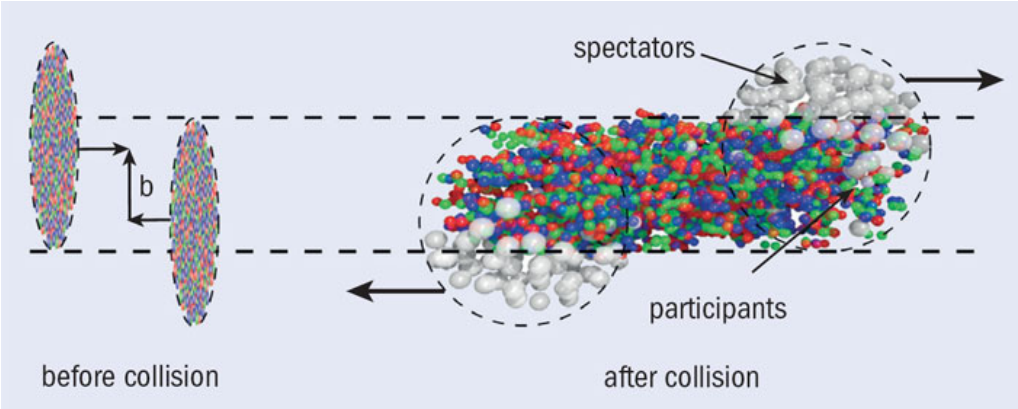

Figure 2.1: Simplified picture of the initial state (before collision) and the final state (after collision) in a heavy-ion collision. In the figure the impact parameter b, the spectators and the participants are indicated. [15]

One of the important variables to study is the *transverse momentum* (p_{T}) of the particles detected,

where transverse means perpendicular to the beamline direction. Defining the beamline to be in the z-direction, the transverse momentum is

$$p_{\mathrm{T}} = \sqrt{p_x^2 + p_y^2} \tag{2.0.1}$$

The transverse momentum indicates how much the reconstructed particles were scattered at the collision point. Characteristically, a hard collision results in a high momentum far off the beam line direction i.e. a high p_{T}. Due to relativistic energies of the participants, it is useful to use the *rapidity* y instead of the standard velocity. The rapidity is defined as

$$y = \frac{1}{2} \ln \left(\frac{E + p_z}{E - p_z} \right) \tag{2.0.2}$$

where E is the energy of a particle, $E = \sqrt{m^2 + \vec{p}^2}$, and p_z is its momentum in the z-direction. The rapidity is a measure of the fraction of momentum in the z-direction carried by the particle. In the center-of-mass frame the region close to $y \approx 0$ is called the *central rapidity* region. The particles in this region are of special interest since they are either new particles resulting from the collision or particles already present in the initial beams that have gone through rescattering processes.

It is however rather difficult to determine the rapidity of highly energetic particles since both the energy and the momentum must be measured. To simplify things one instead measures something closely related to the rapidity, the pseudorapidity η, defined as

$$\eta = \frac{1}{2} \ln \left(\frac{|p| + p_z}{|p| - p_z} \right) = \ln \left(\tan \frac{\theta}{2} \right) \tag{2.0.3}$$

where θ is the angle of the particle's trajectory with respect to the beam line direction (z-direction). The pseudorapidity comes in handy in hadron colliders such as the Large Hadron Collider where the complexity of the collisions makes η easier to measure than y. The high-energy nature of the collisions furthermore implies that η and y are almost identical at high momentum i.e. when $p^2 >> m^2$ for the momentum p and mass m of a particle.

The *impact vector* is defined as the two-dimensional vector connecting the centers of two nuclei participants from different nuclei in the x–y plane. The length of the vector is called the *impact parameter* b, see Fig. 2.1.

The centrality of nucleus-nucleus collision is defined as the percentage of collisions with higher multiplicity or with a greater number of participants. A central or peripheral collision corresponds to a very small or large impact parameter, respectively [14]. Characteristically high-multiplicity or high transverse energy events are from central collisions and low-multiplicity or low-transverse energy events are from peripheral collisions. The most interesting physics is usually found in the most central collisions, with the most participants, highest energies and longest-lived QGP. The difference between central and peripheral collisions in proton-nucleus collisions is not as distinguishable as in the case of nuclei collisions, since the proton is so much smaller than the large nucleus.

3. Heavy-Ion Collisions at the Large Hadron Collider

This section gives a brief overview of the Large Hadron Collider (LHC) situated at CERN near Geneva, Switzerland and one of the experiments conducted there: ALICE. Finally one of the main detectors, the Time Projection Chamber (TPC) at ALICE is introduced.

The Large Hadron Collider

The LHC is the largest and most powerful colliding-beam particle accelerator in the world [16]. The main components of LHC are two 26.7 km circumference synchroton rings, situated 100 m underground below the Swiss/French border. Inside the rings accelerated protons and lead nuclei are collided. Before entering the circular accelerator the protons and nuclei are pre-accelerated with linear accelerators and then fed to the Proton Synchrotron (PS) and the Super Proton Synchrotron (SPS). From the PS and the SPS the particles are transferred to the LHC-rings where they are accelerated up to their collision energies and focused by strong magnetic fields.

The LHC bending magnets' strength has so far allowed a center of mass energy of $\sqrt{s} = 8$ TeV for proton-proton collisions, $\sqrt{s} = 2.76$ TeV for lead-lead collisions and $\sqrt{s} = 5.02$ TeV for proton-lead collisions. An upgrade of the LHC to allow $\sqrt{s} = 13 - 14$ TeV for proton-proton collisions, $\sqrt{s} = 5 - 5.5$ TeV for lead-lead collisions and an energy to be determined for proton-lead collisions, was finalized early 2015.

At the LHC there are four different interaction points for experiments: ATLAS, CMS, LHCb and the one to be further discussed is where the majority of all heavy-ion collision studies at CERN take place: ALICE.

The ALICE experiment

ALICE (A Large Ion Collider Experiment) is the name of the detector dedicated to research on heavy-ion collisions at CERN and more specifically to study the QGP state. Lead nuclei are accelerated in opposite directions in LHC and brought to collide inside the ALICE detector. Following the QGP freeze-out the particles and decay products resulting from the collisions are reconstructed and detected using different parts of the detector.

In total the ALICE detector is 26 m long, 16 m high, 16 m wide and situated 56 m below ground [17]. At the heart of ALICE, closest to the beam line the trackers Inner Tracking System (ITS) and the Time Projection Chamber (TPC) are placed. The TPC is built to reconstruct three-dimensional trajectories of charged particles whereas the ITS is used to determine collision vertex, secondary vertices and improve momentum signals detected in the TPC. Combining the trackers with the other detectors, particles coming out of collisions are identified. Additional to the trackers ALICE consist of an Electromagnetic Calorimeter (EMcal), used for detection of photons and to determine the energy of the outcoming charged particles, a photon spectrometer, a Time-Of-Flight (TOF) detector, a High Momentum Particle IDentification (HMPID) detector and the Transition Radiation Detector (TRD) used to detect electrons. In one of the cylindrical ends of the detector the forward muon spectrometer (muon chambers) is mounted to detect muons. The whole detector is enclosed within a solenoidal magnet creating a 0.5 T [18] magnetic field within the detector. Figure 3.1 shows a schematic layout of the ALICE detector.

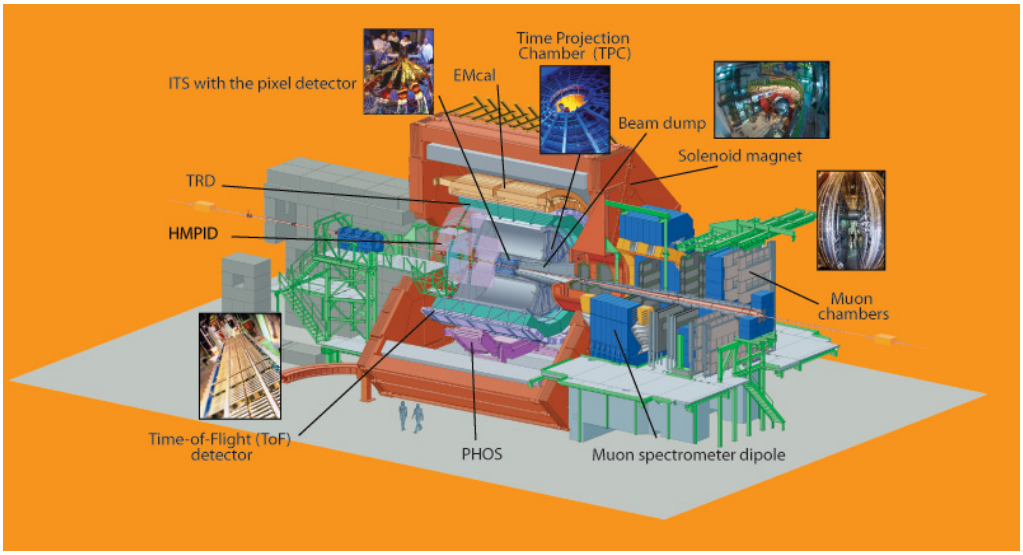

Figure 3.1: Schematic layout of the ALICE experiment. [19]

The detection of J/Ψ particles in heavy ion collisions was one of the main goals of the ALICE experiment during its first run with the LHC, which took place in 2010, with lead beams. ALICE is well-suited to observe J/Ψ production through regeneration of charm quarks with low-p_{T} since it in contrast to other LHC experiments can detect J/Ψ particles down to zero p_{T} with the combination of the TPC and the muon chambers [3].

The Time Projection Chamber

The main tracking detector at the central rapidity of the ALICE detector is the Time Projection Chamber (TPC) used for tracking and identifying particles. The device surrounds the beam pipe and consists of a cylindrical chamber with a volume of 90 m^3. The axis of the chamber is aligned with the LHC beamline and is parallell to the magnetic field. The chamber is filled with a gas mixture of Ne, CO_2 and N_2 and within it an axial electric field is present.

As charged particles pass through the chamber, the gas atoms are ionized and the liberated electrons drift in the electric field. By detecting the electrons with Multi-Wire Proportional Chambers (MWPCs) at each end of the TPC and measuring their drift time, a three-dimensional track image of the ionizing particle is reconstructed. The x–y component is obtained from MWPC data, while the z component is reconstructed using the drift time and the known drift velocity. [18]

The electrons drift towards the end-plane anodes where they are accelerated to higher speeds by the MWPCs. The acceleration causes each electron to create an avalanche of ionized particles and electrons as they ionize the gas further. An electron reaching the anode induces a signal in one or more pads which is registered by the MWPC. As several pads of a single row register the particle, a cluster is created. Due to the limited number of pad rows, a maximum of 159 clusters can be created for each particle. Small dead parts exist between the sectors of anodes where no ionization can be detected.

The average specific energy loss per unit path length of a particle, $\langle \mathrm{d}E/\mathrm{d}x \rangle$, is also measured in the TPC. The specific energy loss is a measure of how much energy the detected particle loses over a distance $\mathrm{d}x$ due to Coulomb interactions with the atoms in the gas and is a statistical process theoretically explained by the Bethe-Bloch function, a function of $\beta\gamma = \frac{p}{m}$:

$$\frac{dE}{dx}(\beta\gamma) = \frac{4\pi N e^4}{mc^4}\frac{1}{\beta^2}z^2\left(\ln\left(\frac{2mc^2}{I}\right)\beta^2\gamma^2 - \beta^2 - \frac{\delta(\beta)}{2}\right) \tag{3.0.1}$$

γ is the Lorentz factor, $\delta(\beta)$ is a density effect correction, I the mean excitation energy of the material, mc^2 the rest energy of the electrons, z the particle charge and N the number of density of the electrons.

The magnetic field present within the TPC causes charged particle to travel in curved trajectories in the x–y plane, also referred to as the *azimuthal plane*, which is used to detemine the momentum of the reconstructed tracks.

Proton–Lead collisions

In 2012, just before the shutdown of the LHC in February the same year, proton–lead (p–Pb) collisions were recorded for the first time in ALICE. Before that, the only available data to compare the lead-lead (Pb–Pb) collisions with was that of proton-proton (p–p) collisions. The run of p–Pb collision lasted only a few weeks, hence there is limited statistics for rare signals available from these collisions.

It is the aim of the p–Pb collision experiments to shed light on the Pb–Pb results by enabling the possible disentanglement between effects of the QGP with those due to the properties of heavy nuclei: Cold Nuclear Matter (CNM) effects. The studies on collisions of p–Pb are motivated as a way of decoupling the CNM effects from that of the QGP by comparing the three different types of collisions.

By definition the CNM effects do not come from the QGP but it has not yet been fully understood how they come into play in the case of QGP physics. It is outside the scope of this thesis to extensively treat CNM effects and therefore the possible effects will only be viewed as a motivation for studying p–Pb collisions. The suppression of J/Ψ has been measured in Pb–Pb collisions at the LHC and it has been found to be stronger at forward rapidity and at high p_{T}, which is in agreement with expectations from recombination models [2]. Hence the p–Pb collisions are needed to quantitatively find the contribution of CNM effects in collisions between heavy nuclei.

4. Analysis Method

The aim is to measure the number of J/Ψ produced in p–Pb collisions in ALICE through an invariant mass analysis. The decay channel studied for the J/Ψ is exclusively the dielectron channel. For this purpose, data from the TPC with information extracted from the detection of charged particles are used. The data consist of events that contain tracks. Each and every track corresponds to one detected particle as reconstructed by the TPC. For the analysis presented here, the invariant mass is calculated from information available in the tracks. The extracted information used is the momentum, specific energy loss ($\mathrm{d}E/\mathrm{d}x$), associated cluster information (n_{eff} and n_{cl}) and ϕ (the azimuthal angle) of the track.

The analysis has been carried out within the ROOT framework [20] using software written in C++. The data are extracted from p–Pb collisions at LHC at the center of mass energy $\sqrt{s} = 5.02$ TeV for all impact parameters and the number of events used is $106.83{\cdot}10^6$.

Before the J/Ψ analysis was carried out, the invariant mass code was tested using data from Pb–Pb collisions with $\sqrt{s} = 2.76$ TeV to see if it was possible to identify a ϕ meson signal (the ϕ meson has a mass of 1.02 GeV/c^2). To do this, the decay channel of the ϕ meson to two Kaons, each having a mass of 0.494 GeV/c^2, was studied. As the ϕ signal was successfully identified, see Fig. 4.1, the invariant mass code was assumed to be working.

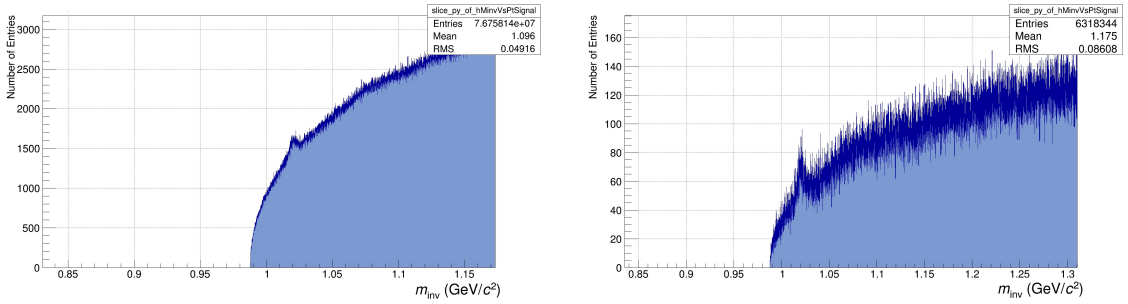

(a) (b)

Figure 4.1: Figure showing the successful identification of the ϕ meson signal: a) the invariant mass distribution for p_{T} 7-8 GeV/c and b) the invariant mass distribution for p_{T} 8 -10 GeV/c.

Track Selection

An initial set of basic cuts was used prior to applying the electron identification criteria. To avoid using fake tracks in the analysis, the ratio between clusters that actually have been observed $\mathrm{n_{eff}}$ and clusters that can be geometrically traversed $\mathrm{n_{cl}}$ is required to be greater than or equal to 0.83 [21]. To be within TPC acceptance ranges, the cut for pseudorapidity is set to $|\eta| < 0.9$ [2] and to remove low-momentum tracks the transverse momentum p_{T} is required to be at least 150 MeV/c.

Electron identification

Particle identification (PID) is performed using the TPC by studying the specific energy loss $\mathrm{d}E/\mathrm{d}x$ distribution as a function of momentum p. In the $\mathrm{d}E/\mathrm{d}x$ vs. p histogram, Fig. 4.2, bands of particles detected in the TPC are visible. TPC tracks consistent with pions, kaons, protons and deuterons are rejected in order to select dielectron (i.e. electron and positron) candidates only. The three intersecting functions show the cuts made on the tracks to select electrons. The enclosed area

by the three functions contains all electron candidates for the J/Ψ decay that were considered. To distinguish between electron pairs and the other particles in the distribution the $\mathrm{d}E/\mathrm{d}x$ vs. p histogram was studied to find suitable conditions. The conditions used were

$$\mathrm{dE/dx} < 95,$$

$$\mathrm{dE/dx} > \frac{50(p^2 + m^2_{\mathrm{proton}})}{m^2_{\mathrm{proton}}},$$

and

$$\mathrm{dE/dx} > 7 \ln\left(1 + \frac{p}{m_{\mathrm{pion}}}\right).$$

where $m_{\mathrm{proton}} = 0.938$ GeV/c^2 and $m_{\mathrm{pion}} = 0.140$ GeV/c^2. The two last conditions given above are simplified Bethe-Bloch-parametrized functions fitted to the specific $\mathrm{d}E/\mathrm{d}x$ distribution of Fig. 4.2.

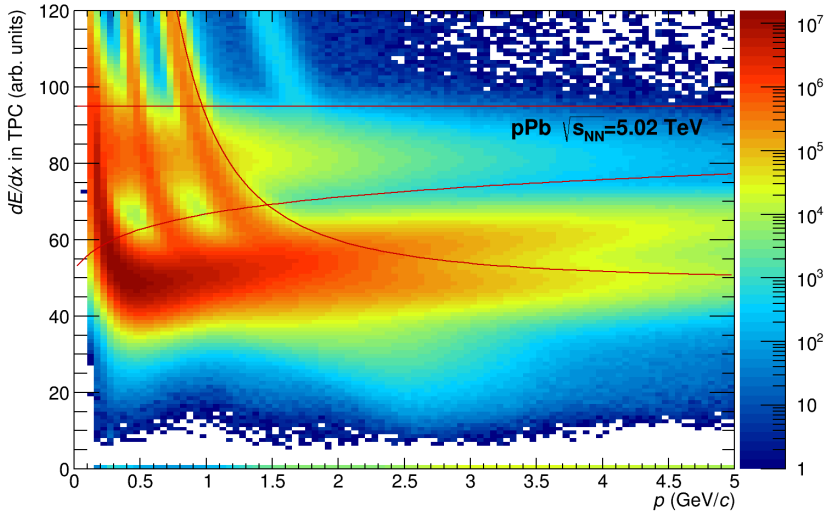

Figure 4.2: Charged particle specific energy loss (dE/dx) as a function of momentum p measured in the TPC in p–Pb collisions. The plot shows three intersecting functions and the used dielectron candidates are within the area enclosed by the functions.

Signal and background estimation

The invariant mass distribution is found by combining every electron or positron candidate with every other electron or positron candidate, calculating the invariant mass as if the two particles had the same origin. Therefore the mass distribution includes a significant combinatorial background. The invariant mass distribution is calculated using the equivalent of Eq. 1.0.2 with the energies of the particles, in natural units (c=1), given by

$$E_1 = \sqrt{m_1^2 + p_1^2}$$

and

$$E_2 = \sqrt{m_2^2 + p_2^2}$$

where p is the total momentum of each particle available in the tracks whereas m_1 and m_2 are the masses of the detected particles. Since the transverse momentum p_{T} and the angle ϕ is also available in the tracks, the components of the momentum are found with

$$p_x = p_{\mathrm{T}} \cos(\phi)$$
$$p_y = p_{\mathrm{T}} \sin(\phi)$$
$$p_z = \sqrt{p^2 - p_{\mathrm{T}}^2}.$$

Finally, the invariant mass can in natural units be calculated

$$m_{\mathrm{inv}} = \sqrt{m_1^2 + m_2^2 + 2E_1E_2 - 2\left(p_{1x}p_{2x} + p_{1y}p_{2y} + p_{1z}p_{2z}\right)}$$

where $m_1 = m_2 = 511$ keV (the known mass of an electron or positron in natural units).

The obtained invariant mass distribution (Unlike-Sign) is shown in Figure 4.3. To estimate the signal, the background (Like-Sign) was estimated to be subtracted from this total invariant mass distribution.

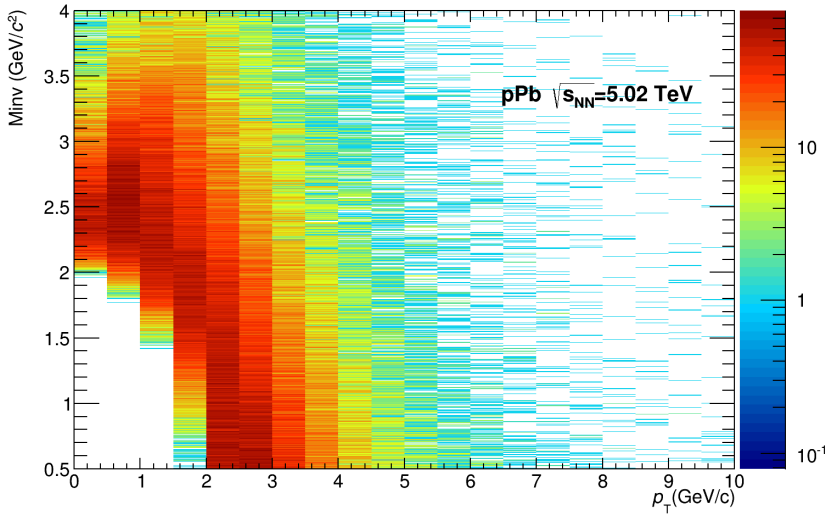

Figure 4.3: Invariant mass distribution as obtained by combining each electron candidate track with every differently charged track (Unlike-Sign), for $0.15 < p_{\mathrm{T}} < 10$ GeV/c.

The background in the invariant mass distribution is estimated from the combination of Like-Sign particles to calculate the J/Ψ particle's invariant mass, (since conservation of charge prohibits such a decay). Possible acceptance difference in the TPC for electrons $(--)$ and positrons $(++)$ were checked for and eventually the total background was subtracted from the total invariant mass distribution of Unlike-Sign paris to find the signal. A comparison was made between twice the geometric mean $2\sqrt{\mathrm{N}_{--}\mathrm{N}_{++}}$ (refered to as the geometric sum further on) and the normal sum $\mathrm{N}_{--} + \mathrm{N}_{++}$. No difference was found, see Table 5.1, and the normal sum was used to calculate the signal.

To study the dependence of the J/Ψ production on p_{T} the invariant mass distribution is considered for different p_{T} intervals separately. Since the combinatorial background is expected to be larger for low p_{T} (due to more tracks at low p_{T}) a larger error in the number of J/Ψ is expected for lower p_{T}. The signal extraction has been performed in five and ten different p_{T} intervals: $p_{\mathrm{T}} < 1.3$,

$1.3 < p_{\mathrm{T}} < 3$, $3 < p_{\mathrm{T}} < 5$, $5 < p_{\mathrm{T}} < 7$ and $7 < p_{\mathrm{T}} < 10$ GeV/c as in [2] and integer p_{T} intervals between 0 and 10 GeV/c, the results are shown in Fig. 4.4 and 4.5. The J/Ψ yields are acquired by counting the number of entries in the invariant mass range $2.92 < \mathrm{m_{inv}} < 3.16$ GeV/c^2 by integration in all three distributions studied: the invariant mass distribution for all combinations (Unlike-Sign) and the two background distributions for electrons and positrons individually. The final signal is estimated to be the Unlike-Sign distribution minus the Like-Sign distribution within the specified m_{inv} range. The uncertainty of the signal extraction is calculated to be the poisson distribution error for the total signal

$$\mathrm{Signal} = \mathrm{N_{Unlike\text{-}Sign}} - \mathrm{N_{Like\text{-}Sign}}$$

where $\mathrm{N_{Like\text{-}Sign}}$ is the normal sum of the two backgrounds. The error is:

$$\sigma = \sqrt{\mathrm{N_{Unlike\text{-}Sign}} + \mathrm{N_{Like\text{-}Sign}}}.$$

The opposite-sign dielectron invariant mass spectra are shown in (blue) for the various p_{T} intervals, compared to the combinatorial background (red) in Fig. 4.4 and 4.5

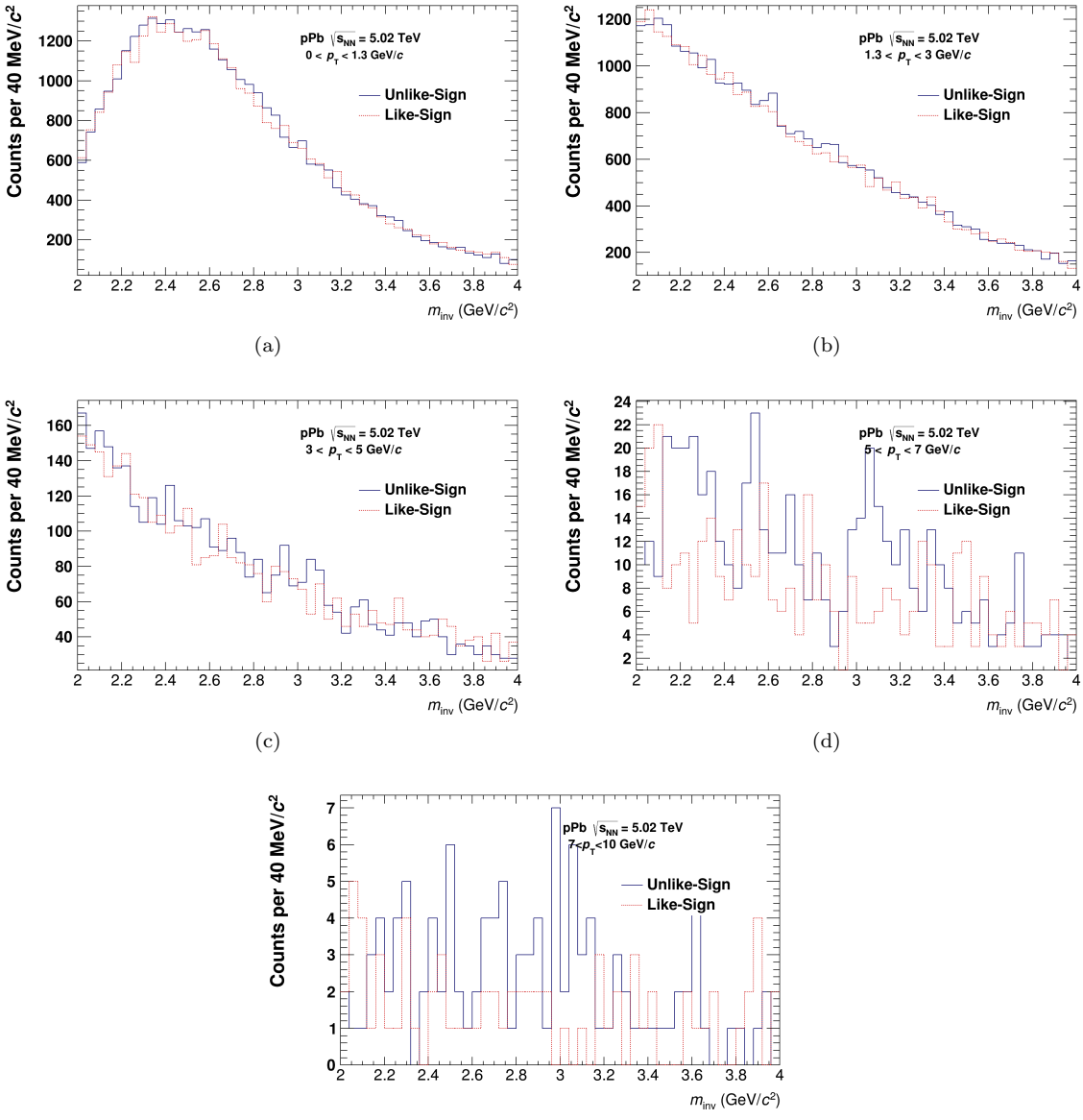

Figure 4.4: Opposite-sign dielectron invariant mass spectra: number of counts per 40 MeV/c^2 for five different p_T intervals. The background shown is the combinatorial background arising from all Like-Sign combinations.

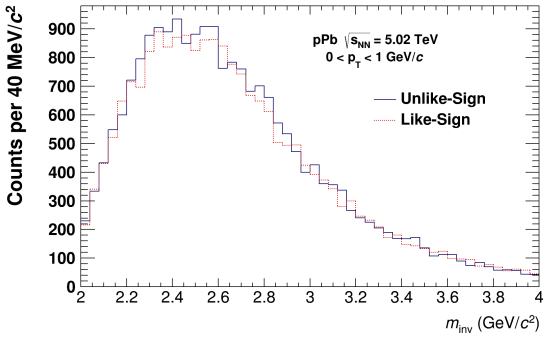
pPb $\sqrt{s_{NN}}$ = 5.02 TeV
0 < p_T < 1 GeV/c
Unlike-Sign
Like-Sign
Counts per 40 MeV/c^2
m_{inv} (GeV/c^2)

(a)

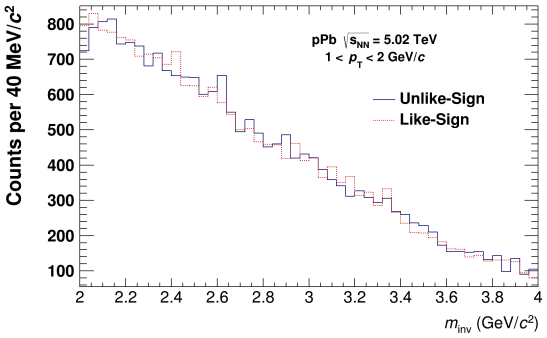
pPb $\sqrt{s_{NN}}$ = 5.02 TeV
1 < p_T < 2 GeV/c
Unlike-Sign
Like-Sign
Counts per 40 MeV/c^2
m_{inv} (GeV/c^2)

(b)

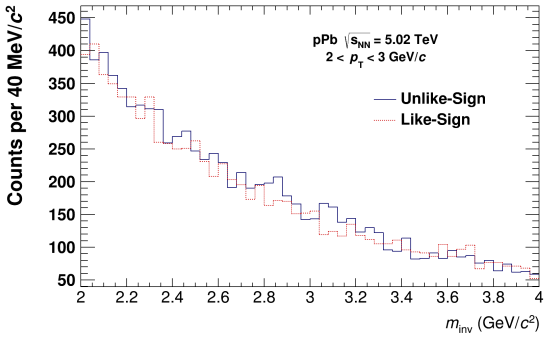
pPb $\sqrt{s_{NN}}$ = 5.02 TeV
2 < p_T < 3 GeV/c
Unlike-Sign
Like-Sign
Counts per 40 MeV/c^2
m_{inv} (GeV/c^2)

(c)

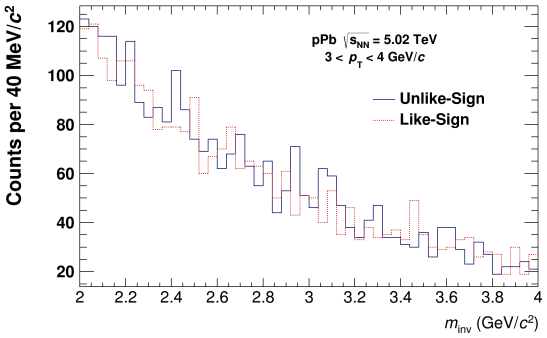
pPb $\sqrt{s_{NN}}$ = 5.02 TeV
3 < p_T < 4 GeV/c
Unlike-Sign
Like-Sign
Counts per 40 MeV/c^2
m_{inv} (GeV/c^2)

(d)

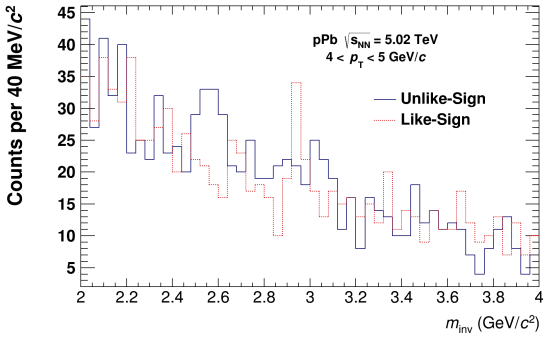
pPb $\sqrt{s_{NN}}$ = 5.02 TeV
4 < p_T < 5 GeV/c
Unlike-Sign
Like-Sign
Counts per 40 MeV/c^2
m_{inv} (GeV/c^2)

(e)

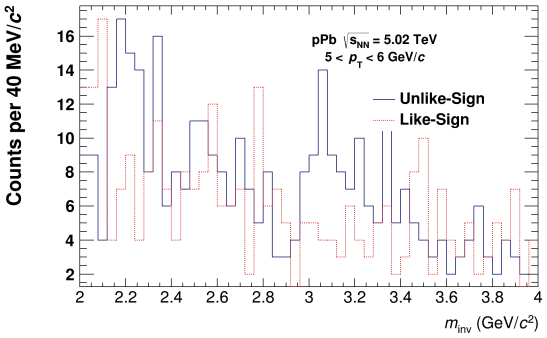
pPb $\sqrt{s_{NN}}$ = 5.02 TeV
5 < p_T < 6 GeV/c
Unlike-Sign
Like-Sign
Counts per 40 MeV/c^2
m_{inv} (GeV/c^2)

(f)

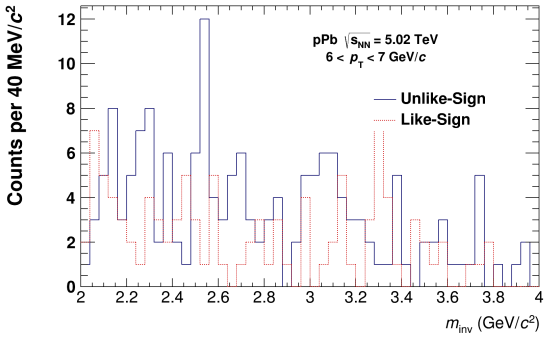
pPb $\sqrt{s_{NN}}$ = 5.02 TeV
6 < p_T < 7 GeV/c
Unlike-Sign
Like-Sign
Counts per 40 MeV/c^2
m_{inv} (GeV/c^2)

(g)

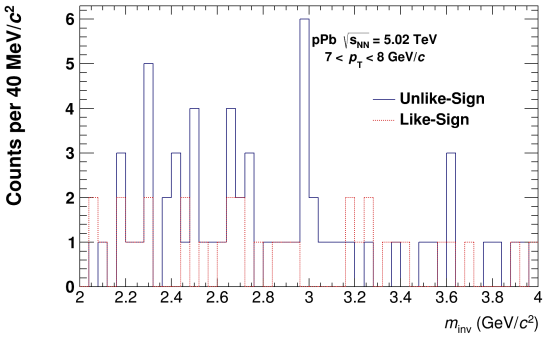
pPb $\sqrt{s_{NN}}$ = 5.02 TeV
7 < p_T < 8 GeV/c
Unlike-Sign
Like-Sign
Counts per 40 MeV/c^2
m_{inv} (GeV/c^2)

(h)

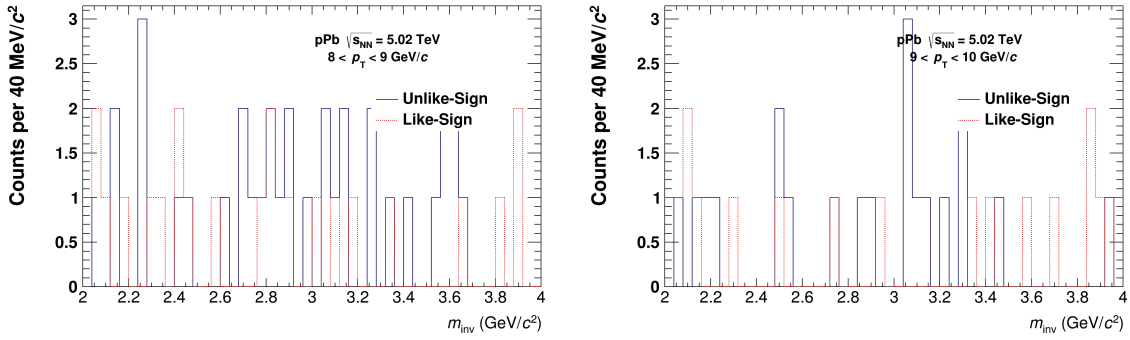

(i) (j)

Figure 4.5: Opposite-sign dielectron invariant mass spectra: number of counts per 40 MeV/c^2 for integer p$_T$ intervals from 0 to 10 GeV/c. The background shown is the combinatorial background arising from all Like-Sign combinations.

To estimate the centrality dependence of the J/Ψ production the J/Ψ yield was measured for different ranges of the number of tracks per event (since a more central collision results in a higher multiplicity, i.e. more tracks per event). Figure 4.6 shows the total number of tracks per event distribution for all events in the data used. The J/Ψ yield was calculated for integer p_{T} intervals from 0 to 10 GeV/c for three different centralities estimated by the number of tracks per event: peripheral collisions (tracks/event $<$ 20) , mid-peripheral-central collisions (20 $<$ tracks/event $<$ 40) and central collisions (tracks/event $>$ 40).

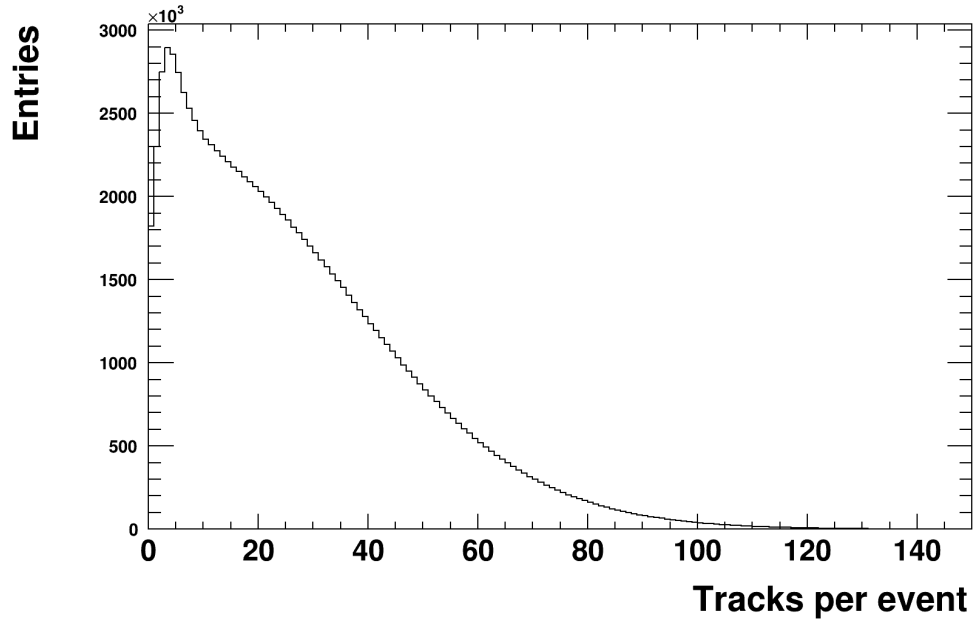

Figure 4.6: Entries for the number of tracks per event for the p–Pb data used.

5. Results

The number of J/Ψ estimated for the different p_{T} intervals are given in Table 5.1. In total, the number of J/Ψ for $p_{\mathrm{T}} > 3$ GeV/c in the range $2.92 < \mathrm{m}_{inv} < 3.16$ GeV/c^2 is 127 $\pm$ 31. As seen in Fig. 5.1 and 5.2 there are cases where the J/Ψ yields are below zero (unphysical) and hence resulting in lower integrated yields. These unphysical yields are, as shown in Table 5.1, not significant, less than one σ away from zero. The three p_{T} intervals where the non-significant signal estimate is negative are thus ranges where no signal is viewed above the background.

Fig. 5.1 and 5.2 show the invariant mass distributions when the Like-Sign distribution have been subtracted from the Unlike-Sign distribution. The figures indicate the invariant mass range $2.92 < m_{\mathrm{inv}} < 3.16$ GeV/c^2 integrated to calculate the J/Ψ yield. Examination of Fig. 5.1 and 5.2 shows that for low p_{T} the number of J/Ψ candidates may be high but is also more uncertain, for the significant yields found. For higher p_{T} the yields found are lower but with a smaller uncertainty, see e.g. Fig. 5.4. The uncertainty grows for low p_{T} as expected, since there are more counts both for the total distribution and the background for the low p_{T} intervals as compared to the high p_{T} intervals. For the p_{T} ranges $5 < p_{\mathrm{T}} < 6$, $5 < p_{\mathrm{T}} < 7$ and $7 < p_{\mathrm{T}} < 10$ GeV/c the most significant J/Ψ yields are found, with a significance of at least 3.

Table 5.1 also shows that the background estimates (geometric vs. normal) of combined electrons and positrons are to a good approximation the same and as shown in Fig. 5.3 and 5.4 the yield goes down with p_{T}.

As seen in Fig. 5.5 there is less statistics available for the peripheral collisions. Since the number of tracks per event is low for a more peripheral collision there is a lower number of available electron candidates, and thus a lower yield of J/Ψ candidates. For the mid-peripheral-central collisions, Fig. 5.6, there are more tracks available which results in a higher yield than for the peripheral collisions. However, the more central collisions also result in a greater background due to the many tracks available. Figure 5.7 shows the yield for central collisions where a lot more tracks per event are available, hence more electron candidates to calculate the J/Ψ yield. Here many more tracks per event result in a high background, especially for low p_{T}. The yield estimates found in Figure 5.4 and 5.7 look quite similar, showing that the total J/Ψ yield calculated comes mostly from central collisions where each event contain more tracks.

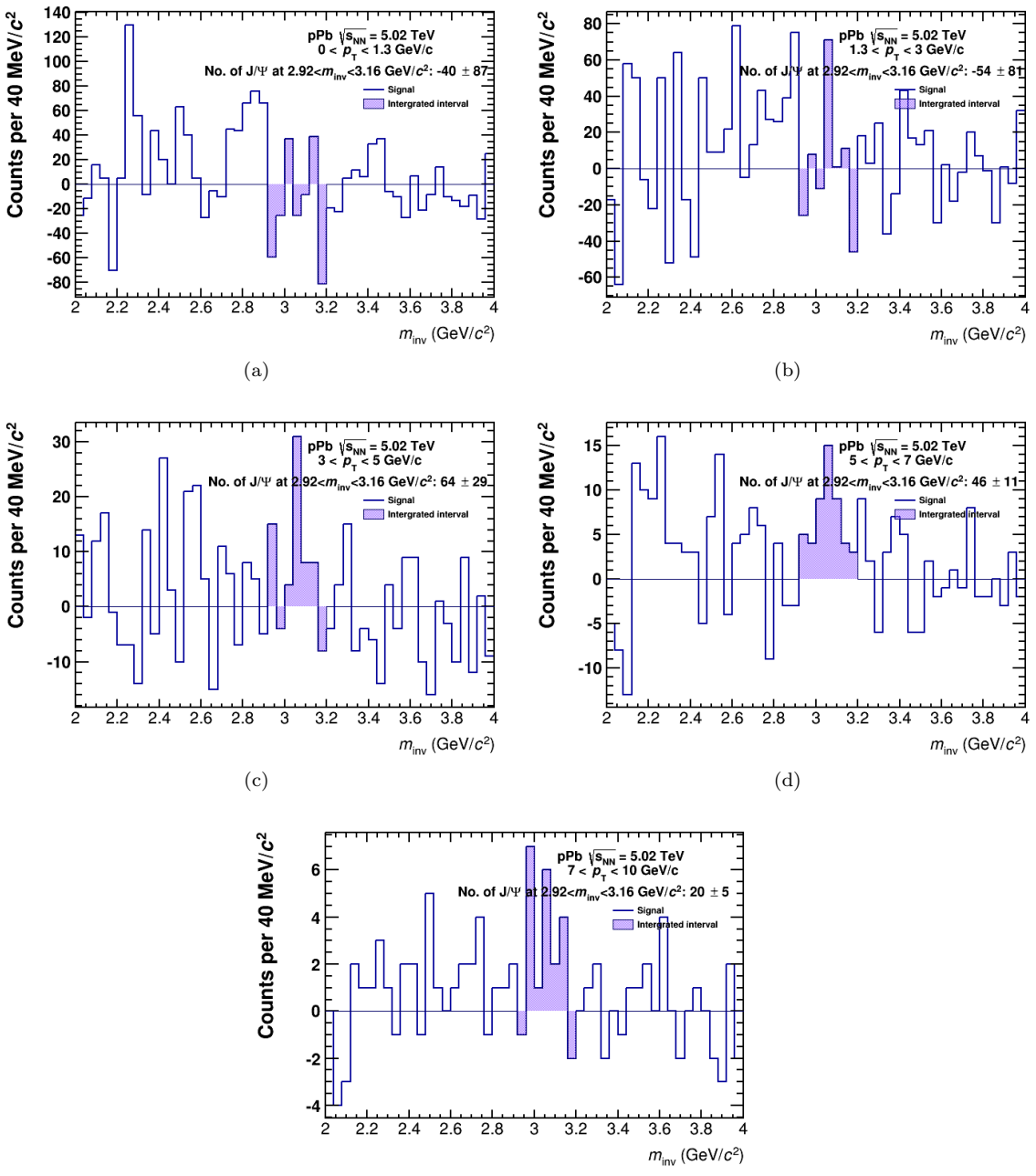

Figure 5.1: Unlike-Sign dielectron invariant mass spectra: number of counts per 40 MeV/c^2 for five different p_T intervals, as in [2] with the background subtracted from the foreground. The integrated range 2.92 < m_{inv} <3.16 GeV/c^2 is shown and the number of J/Ψ particles calculated after background subtraction.

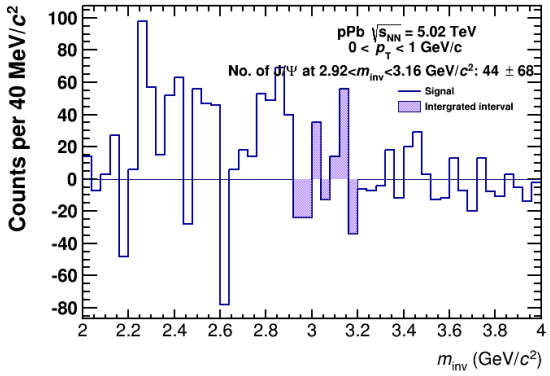
pPb $\sqrt{s_{NN}}$ = 5.02 TeV
0 < p_T < 1 GeV/c
No. of J/Ψ at 2.92<m_{inv}<3.16 GeV/c^2: 44 ± 68
Signal
Intergrated interval
Counts per 40 MeV/c^2
m_{inv} (GeV/c^2)

(a)

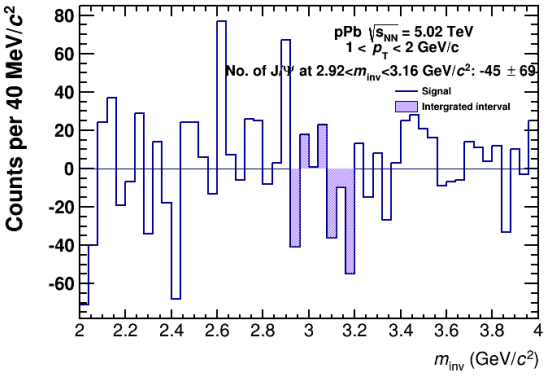
pPb $\sqrt{s_{NN}}$ = 5.02 TeV
1 < p_T < 2 GeV/c
No. of J/Ψ at 2.92<m_{inv}<3.16 GeV/c^2: -45 ± 69
Signal
Intergrated interval
Counts per 40 MeV/c^2
m_{inv} (GeV/c^2)

(b)

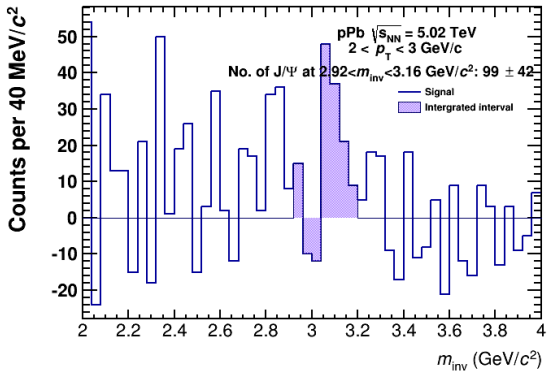
pPb $\sqrt{s_{NN}}$ = 5.02 TeV
2 < p_T < 3 GeV/c
No. of J/Ψ at 2.92<m_{inv}<3.16 GeV/c^2: 99 ± 42
Signal
Intergrated interval
Counts per 40 MeV/c^2
m_{inv} (GeV/c^2)

(c)

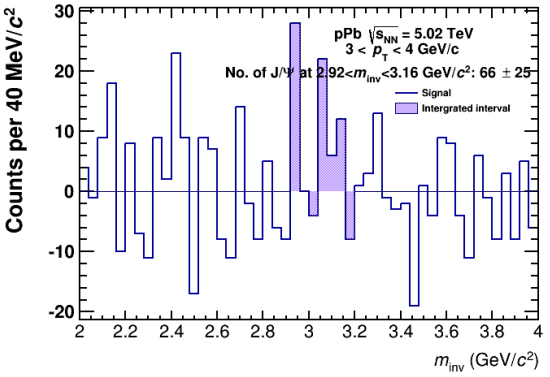
pPb $\sqrt{s_{NN}}$ = 5.02 TeV
3 < p_T < 4 GeV/c
No. of J/Ψ at 2.92<m_{inv}<3.16 GeV/c^2: 66 ± 25
Signal
Intergrated interval
Counts per 40 MeV/c^2
m_{inv} (GeV/c^2)

(d)

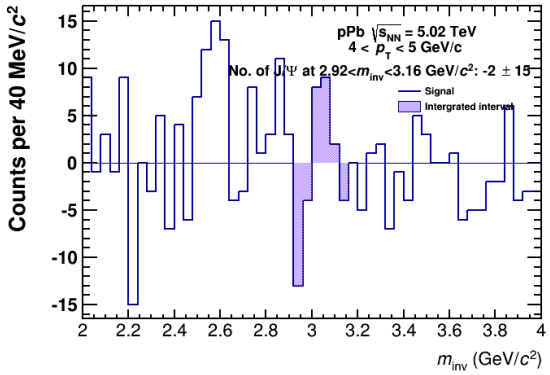
pPb $\sqrt{s_{NN}}$ = 5.02 TeV
4 < p_T < 5 GeV/c
No. of J/Ψ at 2.92<m_{inv}<3.16 GeV/c^2: -2 ± 15
Signal
Intergrated interval
Counts per 40 MeV/c^2
m_{inv} (GeV/c^2)

(e)

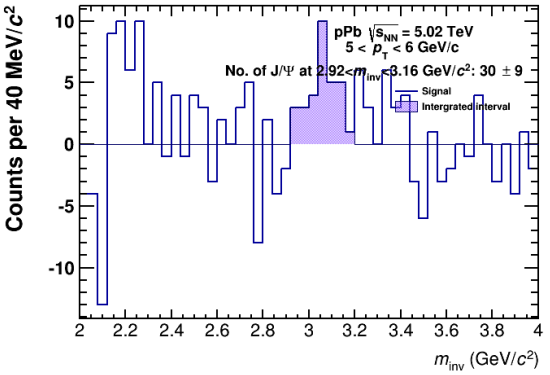
pPb $\sqrt{s_{NN}}$ = 5.02 TeV
5 < p_T < 6 GeV/c
No. of J/Ψ at 2.92<m_{inv}<3.16 GeV/c^2: 30 ± 9
Signal
Intergrated interval
Counts per 40 MeV/c^2
m_{inv} (GeV/c^2)

(f)

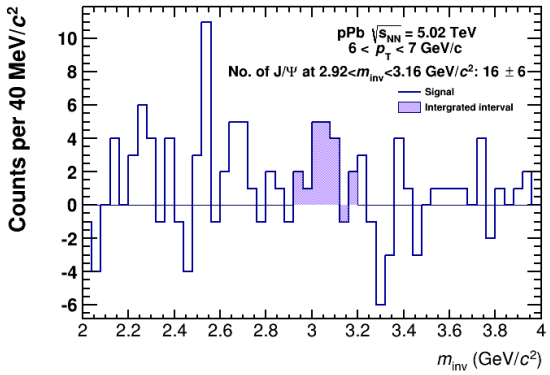
pPb $\sqrt{s_{NN}}$ = 5.02 TeV
6 < p_T < 7 GeV/c
No. of J/Ψ at 2.92<m_{inv}<3.16 GeV/c^2: 16 ± 6
Signal
Intergrated interval
Counts per 40 MeV/c^2
m_{inv} (GeV/c^2)

(g)

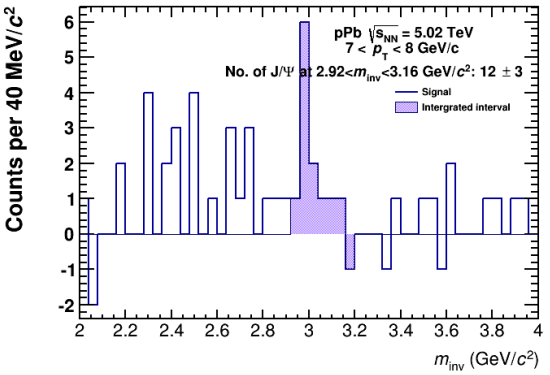
pPb $\sqrt{s_{NN}}$ = 5.02 TeV
7 < p_T < 8 GeV/c
No. of J/Ψ at 2.92<m_{inv}<3.16 GeV/c^2: 12 ± 3
Signal
Intergrated interval
Counts per 40 MeV/c^2
m_{inv} (GeV/c^2)

(h)

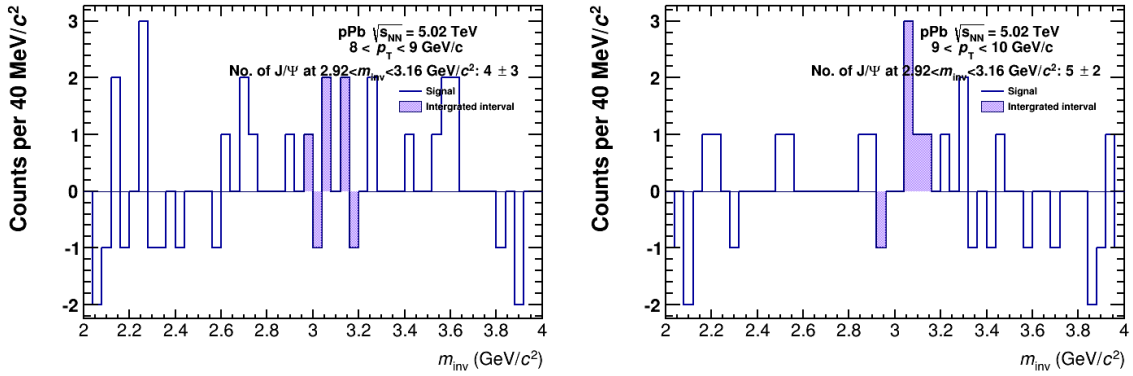

(i) (j)

Figure 5.2: Unlike-Sign dielectron invariant mass spectra: number of counts per 40 MeV/c^2 for integer p_{T} intervals from 0 to 10 GeV/c with the background subtracted from the foreground. The integrated range $2.92 < \mathrm{m}_{inv} < 3.16$ GeV/c^2 is shown and the number of J/Ψ particles calculated after background subtraction.

Table 5.1: Summary of the results on the yields of Unlike-Sign Counts, the electron and poistron background summed to find the total number of Like-Sign pairs and the Signal, for the various p_{T} intervals, for all centralities. The uncertainty and significance is indicated.

p_{T} -range (GeV/c)	Unlike-Sign Counts	Bkgd (++)	Bkgd (−−)	Like-Sign Counts (Geometrical Sum)	Like-Sign Counts (Normal Sum)	Signal	Uncertainty σ	Significance Signal/σ
$0 < p_{\mathrm{T}} < 1.3$	3786	1947	1880	3826	3827	-41	87	-0.46
$1.3 < p_{\mathrm{T}} < 3$	3276	1629	1593	3222	3222	54	81	0.68
$3 < p_{\mathrm{T}} < 5$	452	216	174	388	390	62	29	2.2
$5 < p_{\mathrm{T}} < 7$	80	15	19	34	34	46	11	4.2
$7 < p_{\mathrm{T}} < 10$	23	3	1	4	4	19	5	4
$0 < p_{\mathrm{T}} < 1$	2349	1173	1132	2305	2305	44	68	0.65
$1 < p_{\mathrm{T}} < 2$	2359	1216	1188	2404	2404	-45	69	-0.65
$2 < p_{\mathrm{T}} < 3$	917	413	405	818	818	99	42	2.4
$3 < p_{\mathrm{T}} < 4$	336	152	120	270	272	64	25	2.6
$4 < p_{\mathrm{T}} < 5$	116	64	54	118	118	-2	15	-0.13
$5 < p_{\mathrm{T}} < 6$	52	10	12	22	22	30	9	3.3
$6 < p_{\mathrm{T}} < 7$	28	5	7	12	12	16	6	2.7
$7 < p_{\mathrm{T}} < 8$	12	1	0	0	1	11	4	3
$8 < p_{\mathrm{T}} < 9$	6	1	1	2	2	4	3	1.3
$9 < p_{\mathrm{T}} < 10$	5	1	0	0	1	5	2	2.5

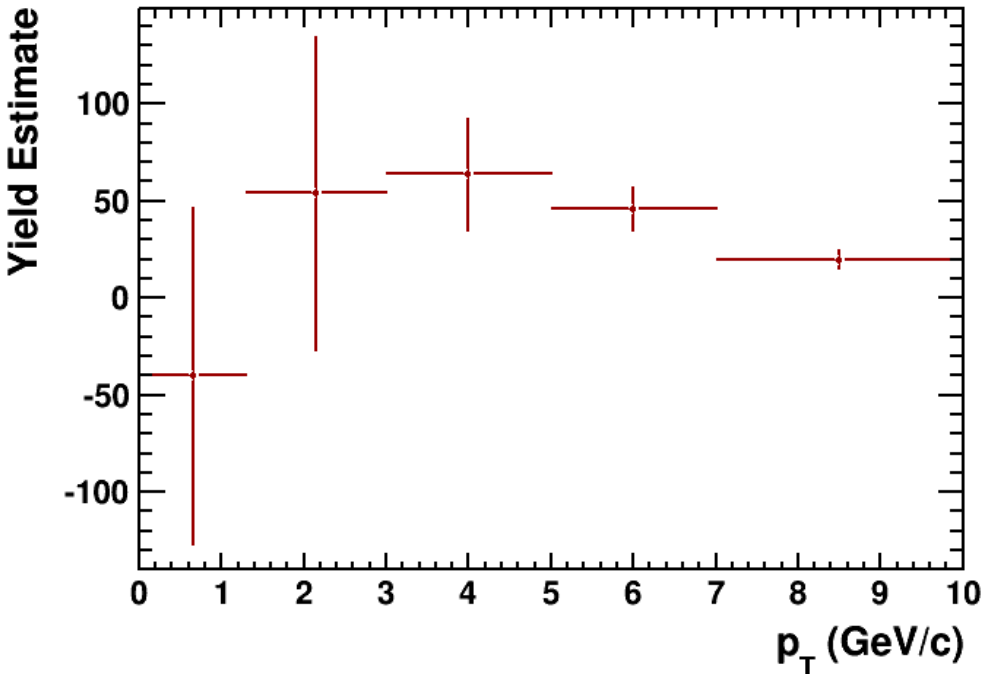

Figure 5.3: Number of estimated J/Ψ particles per p_{T} interval, as in [2].

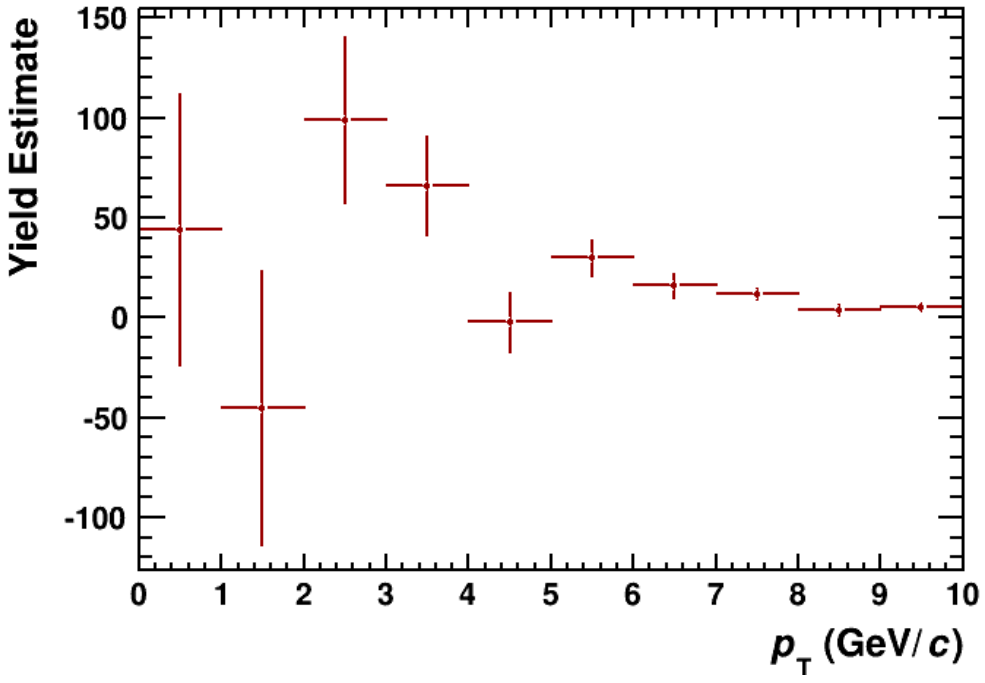

Figure 5.4: Number of estimated J/Ψ particles per integer p_{T} interval.

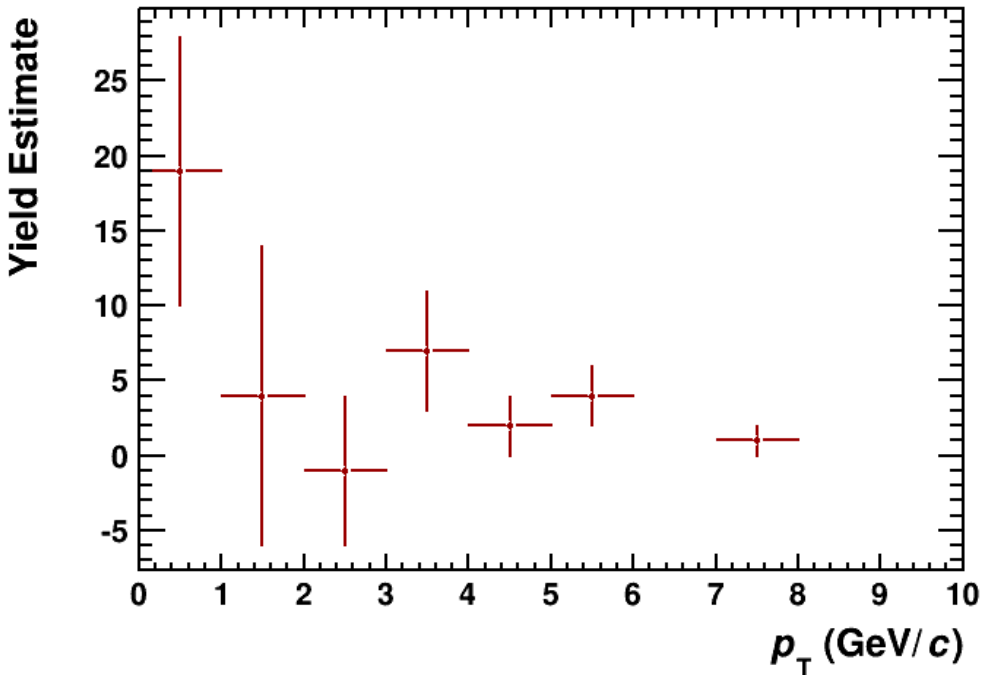

Figure 5.5: Number of estimated J/Ψ particles per integer p_T interval for peripheral collisions (Number of tracks per event < 20)

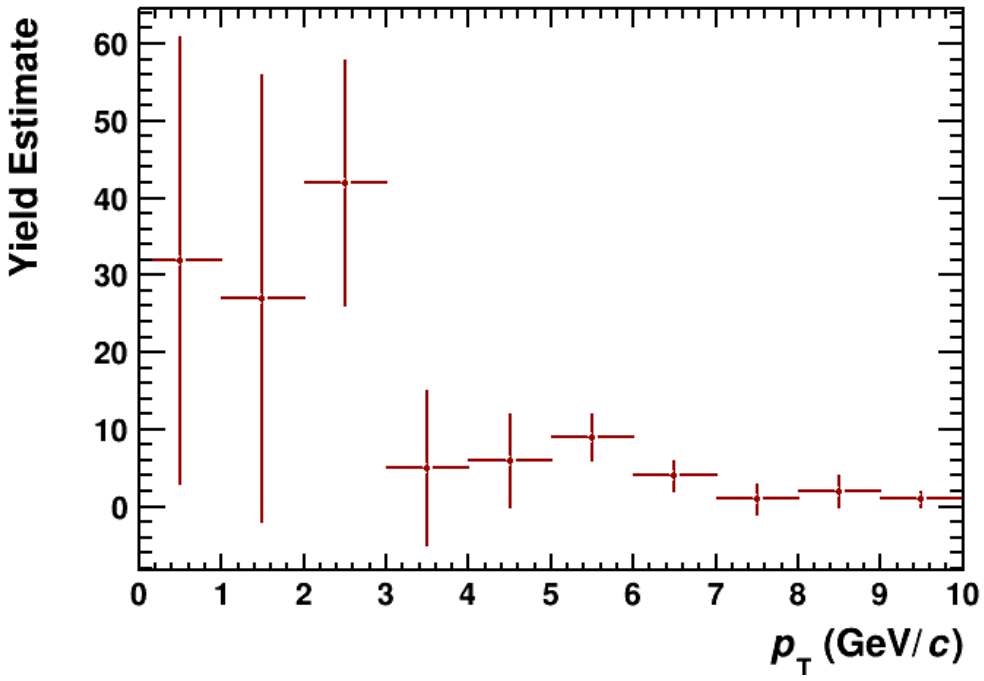

Figure 5.6: Number of estimated J/Ψ particles per integer p_T interval for mid-central collisions (Number of tracks per event > 20 and < 40)

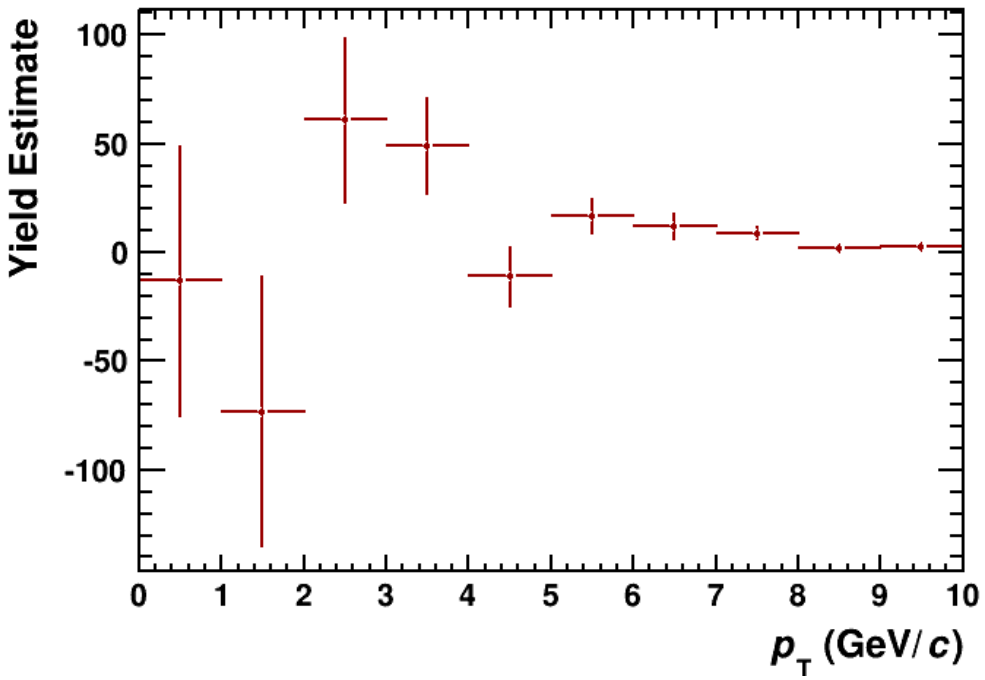

Figure 5.7: Number of estimated J/Ψ particles per integer p_{T} interval for central collisions (Number of tracks per event > 40)

6. Conclusions and Discussion

The question of whether a QGP state is created in p–Pb collisions will remain unanswered here. It is however possible to say that a study of the production of J/Ψ particles is possible using the TPC, especially at high p_{T}. Contrary to the statement of the advantage of using the ALICE detector for the detection of low p_{T} J/Ψ in [sec. 3.2, p. 12] , it was here not possible to distinguish any significant counts of J/Ψ for low p_{T}. To make this possible a cleaner electron track sample would be needed, which was not possible to obtain with the data files available to me. The electron candidates used for the above analysis do not only contain electrons but also other hadrons such as deutrons and pions. Even if all electrons were to be found in the data sample most of them are not from J/Ψ decay. Electrons from other decays than the J/Ψ are due to pions decaying into photons that annihilate to electrons, but also from heavy quark decay, such as the D^0 meson decay to electrons.

Significant yield in the analysis is only observed for p_{T} from 2-3 GeV/c to 10 GeV/c. To draw any further conclusions regarding a J/Ψ suppression or enhancement in the p–Pb collisions comparisons with yields in p–p and Pb–Pb collisions have to be made. To get the full scope of such a comparison, more thorough analysis on p–Pb data is needed.

The analysis here calls for a couple of improvements for a correct characterization on the number of J/Ψ produced in the p–Pb collisions. In the following such improvements are listed.

- The electrons could be more cleanly separated from the large background of pions, kaons and protons through a better PID. A more efficient PID would yield a cleaner electron identification which in turn would result in a better characterization of the Unlike-Sign and Like-Sign counts. This would probably improve the counts of J/Ψ in lower p_{T} ranges where most of the collected data are from. A better electron identification could be done using the TPC plus the Electromagnetic Calorimeter (EMCal) and the Transition Radiation Detector (TRD) detectors of ALICE. At the time of the collection of the above used data of p–Pb collisions the TRD was not fully in use, but however would in the future enable a more precise momentum measurement of the electrons detected in the trackers.

- Efficiency and and acceptance correction factors would need to be estimated and applied to the above analysis to obtain cross-sections.

- The background estimate could also be be improved with a careful mixed-event study, which should reduce the statistical uncertainty of the background beyond what is possible with the Unlike-Sign estimate. Performing a full mixed-event study was however considered beyond the scope of this thesis.

- To account for the full production of J/Ψ in the p–Pb data the study of the invariant mass distribution should also be compared to the dimuon decay channel of J/Ψ. Such an analysis can however only account for muons in the forward rapidity, due to the location of the muon chambers as shown in Fig. 3.1.

- For a better estimate of the J/Ψ production's dependence on centrality an independent detector should be used to caulculate the centrality of each event. Since all data tracks used in the above analysis come from the TPC the estimated centrality dependence of the J/Ψ yield somewhat biased.

Acknowledgements

I would like to thank my supervisor David Silvermyr for introducing me to the study on QGP and for all the support, help and feedback during the whole project. Many thanks to Tuva Richert, Vytautas Vislavičius and Martin Ljunggren for sharing their invaluable expertise on both particle physics and programming. I thank Peter Christiansen for the ROOT script that I've used as a basis for my analysis and I thank Fabian Thiele for sharing some of the code he used for his Master Project. Thank you Adam Johansson and finally great thanks to Anders Oskarsson and Anders Floderus for sharing their knowledge on particle physics and giving me feedback on this thesis.

Bibliography

[1] ALICE. Heavy ions and quark-gluon plasma @http://home.web.cern.ch/about/physics/heavy-ions-and-quark-gluon-plasma;. Last visited on 2015-05-08.

[2] Adam J, et al. Rapidity and transverse-momentum dependence of the inclusive J/ψ nuclear modification factor in p-Pb collisions at $\sqrt{s_{\mathbf{NN}}} = 5.02$ TeV. 2015;.

[3] ALICE. The mystery of the J/Psi @http://aliceinfo.cern.ch/Public/en/Chapter1/results.html;. Last visited on 2015-05-10.

[4] B R Martin GS. Particle Physics. 3rd ed. John Wiley & Sons; 1993.

[5] Iancu E. QCD in heavy ion collisions. 2014;p. 197–266.

[6] Fermilab. The science of matter, space and time@ http://www.fnal.gov/pub/science/inquiring/matter/madeof/; 2014. Last visited on 2015-05-14.

[7] Chaudhuri AK. A short course on Relativistic Heavy Ion Collisions. 2012;.

[8] Cernpress. Heavy-ion collisions, the quark-gluon plasma, and quantum chromodynamics @http://press.web.cern.ch/backgrounders/heavy-ion-collisions-quark-gluon-plasma-and-quantum-chromodynamics;. Last visited on 2015-04-28.

[9] Harris JW, Muller B. The Search for the quark - gluon plasma. AnnRevNuclPartSci. 1996;46:71–107.

[10] Courier C. First results from proton–lead colliding beams @http://cerncourier.com/cws/article/cern/51533;. Last visited on 2015-05-17.

[11] Group PD. J/Psi(1S) DECAY MODES @ http://pdg.lbl.gov/2010/listings/rpp2010-list-J-psi-1S.pdf;. Last visited on 2015-05-14.

[12] Ruiz R. The particle with two names: The J/Ψ Vector Meson @ http://www.quantumdiaries.org/2014/08/06/jpsi;. Last visited on 2015-04-29.

[13] Matsui T, Satz H. J/ψ Suppression by Quark-Gluon Plasma Formation. PhysLett. 1986;B178:416.

[14] Florowski) W. Phenomenology of Ultra-Relativistic Heavy-Ion Collisions. World Scientific Publishing; 2010.

[15] Courier C. The Alice Experiment @ http://www.cerncourier.com;. Last visited on 2015-05-14.

[16] LHC. The Large Hadron Collider @ http://home.web.cern.ch/topics/large-hadron-collider;. Last visited on 2015-04-29.

[17] ALICE. ALICE detects quark-gluon plasma, a state of matter thought to have formed just after the big bang @http://home.web.cern.ch/about/experiments/alice;. Last visited on 2015-05-14.

[18] ALICE. The ALICE Time Projection Chamber (TPC) @http://aliceinfo.cern.ch/ Public/en/Chapter2/Chap2TPC.html;. Last visited on 2015-05-10.

[19] CERN. The LHC in pictures @https://bigscience.web.cern.ch;. Last visited on 2015-05-14.

[20] ROOT. @https://root.cern.ch/drupal/;. Last visited on 2015-06-02.

[21] Thiele FAJ. Test background estimates for resonance measurements using a combination of mixed events and like sign pairs; 2015. Student Paper.